Measurement Based Simulation of Microscope Deviations for Evaluation of Stitching Algorithms for the Extension of Fourier - based Alignment

Florian Engelke*[a], Markus Kästner[a], Eduard Reithmeier[a]
[a]Institute of Measurement and Automatic Control, Leibniz Universität Hannover, Nienburger Str.17, 30167 Hannover, Germany

ABSTRACT

Image stitching is a technique used to measure large surface areas with high resolution while maintaining a large field of view. We work on improving data fusion by stitching in the field of microscopic analysis of technical surfaces for structures and roughness. Guidance errors and imaging errors such as noise cause problems for seamless image fusion of technical surfaces. The optical imaging errors of 3D Microscopes, such as confocal microscopes and white light interferometers, as well as the guidance errors of their automated positioning systems have been measured to create a software to simulate automated measurements of known surfaces with specific deviations to test new stitching algorithms. We measured and incorporated radial image distortion, interferometer reference mirror shape deviations, statistical noise, drift of the positional axis, on-axis-accuracy and repeatability of the used positioning stages and misalignment of the CCD-Chip with respect to the axes of motion. We used the resulting simulation of the measurement process to test a new image registration technique that allows for the use of correlation of images by fast fourier transform for small overlaps between single measurements.

Keywords: stitching, data fusion, image acquisition, 3D microscopy, white-light interferometry, confocal microscopy, image alignment

1. INTRODUCTION

The creation of high resolution images using white light interferometers (WLI) and confocal microscopes (CM) is a technique often used in the inspection of technical surfaces [1-5]. The image acquisition process of the entire measurement is subject of a great number of disturbing influences. This covers errors in the creation of single measurements, the shortcomings in the positioning systems used for sensor to sample translation and the algorithms to for registration and fusion of the measurement data. To accurately research the influence of the various error sources we developed a simulation that encompasses the creation of simulated surfaces, the measurement by WLI and CM and the translation of the sample by simulated positioning systems. To base our simulated error sources on reality we performed measurements of the systematic and statistical errors of the microscopes available to us. We used the simulation for the evaluation of an image registration algorithm we developed using measurement sets with known deviations.

2. OPTICAL AND COMPUTATIONAL MEASUREMENT ARTIFACTS

As the surface measurements are all generated by the same optical and computational instruments it is necessary to characterize their errors occurring during imaging the surface. We measured and modeled the radial distortion by the lens system, the statistical deviations in height measurements and the errors introduced to the measurement by imperfect Mirau reference mirrors in WLI imaging.

*florian.engelke@imr.uni-hannover.de ; phone +49 511 762 4278; fax +49 511 762 3234; imr.uni-hannover.de

Modeling Aspects in Optical Metrology IV, edited by Bernd Bodermann, Karsten Frenner, Richard M. Silver,
Proc. of SPIE Vol. 8789, 87890G · © 2013 SPIE · CCC code: 0277-786X/13/$18 · doi: 10.1117/12.2020595

Downloaded From: http://proceedings.spiedigitallibrary.org/ on 07/11/2013 Terms of Use: http://spiedl.org/terms

2.1 Distortions

The corrections of lens distortions are critical for the successful alignment and fusion of overlapping measurements. We characterized the objectives of our microscopes by measuring chessboard surfaces on a microscope calibration chip. Based on the positions of the corners of the squares we optimized the radial distortion transformation (eq. 1) [6,7]. It states the position of a point on the image is a function of its real coordinates and its distance to the optical axis. The transformation is expanded in orders of the dependency on the radial position. The criteria we used for optimization is the uniformity of the vector grid of the chessboard. In an ideal chessboard the sides of all squares have equal lengths, the edges along one direction are all parallel with respect to one another and perpendicular to the edges in the second direction. After guessing the position of the optical axis based on the curvature of the grid a successive optimization for increasingly higher order transformations is started until the error function converges.

$$\begin{pmatrix} x' \\ y' \end{pmatrix} = \begin{pmatrix} x \\ y \end{pmatrix} \cdot \sum_{n=0}^{\infty} k_n \left[\left((x-x_c)^2 + \left(y-y_c\right)^2 \right) / R^2 \right]^n \quad , \quad k_0 = 1 \qquad (1)$$

Here k_n are the expansion coefficients, x_c and y_c the coordinates of the optical center, R the radius of the minimal bounding circle of the image with center at the image center.

We analyzed the capabilities of our algorithm based on simulated chessboard surfaces and transformed them with known distortion parameters and evaluated the difference of the edge positions before distortion and after correction. For distortions in the range measured for our objective lenses we achieved remaining position errors in the range of one pixel. For a successful operation of our algorithm it is necessary that the distance between the image center and the position the optical axis is below 40% of the radius of the minimum bounding circle, centered at the image center, of the image. Figure 1 shows a distorted chessboard measurement and equivalent image portions before and after distortion correction.

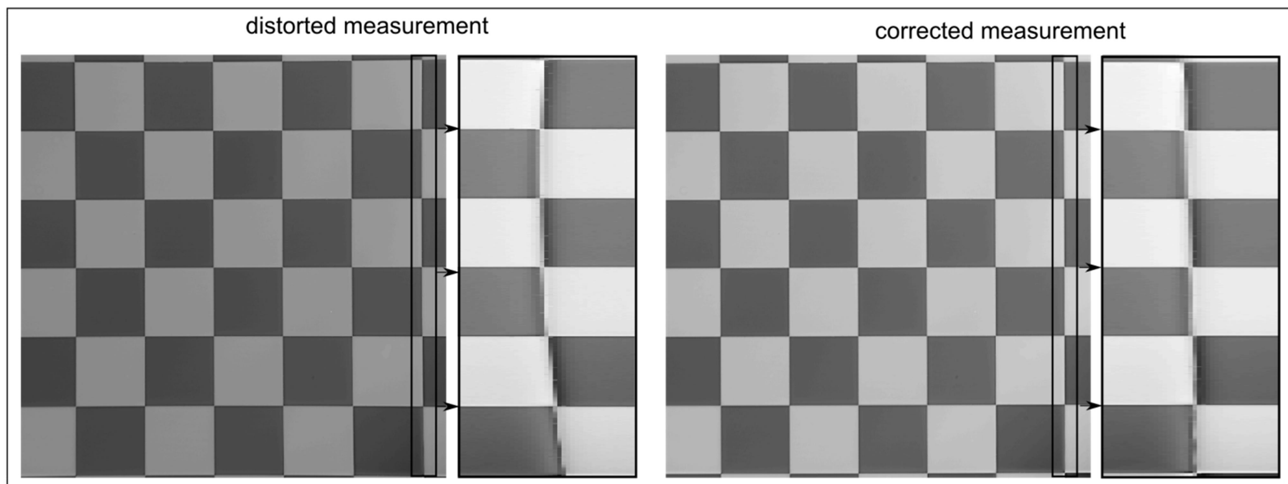

Figure 1: distorted measurement of chessboard with 50 µm pitch by a confocal microscope, exhibiting pincushion distortion (left), after correction by square grid optimization (right)

2.2 Measurement Noise

The sources of noise in WLI and CM measurements are hard to identify as a number of influences can be its cause. The noise of the actual CCD-chip used in the microscope is of course one of the sources, but as the stack images are only used for the evaluation by a fitting function it is only a secondary source, along with quantization, short time illumination changes, faulty z-position at the time of measurement and flaws of the fit algorithm used for stack evaluation. For now we are only interested in the actual noise characteristic of the datasets of commercial WLI and CM’s and not the influences of the distinct error sources. To identify the noise we measured a mirror standard about one hundred times with a low resolution objective lens, to minimize the effects of lateral drift. After height drift correction we plotted a

Downloaded From: http://proceedings.spiedigitallibrary.org/ on 07/11/2013 Terms of Use: http://spiedl.org/terms

histogram for the deviation of each pixel from the median height value of that pixel. We found that the noise can be described roughly by a Gaussian distribution, but especially for the WLI the distribution contained an asymmetric part (Figure 2). To make maximum use of these measurements we use the measurement data as a noise distribution for our virtual microscopes.

2.3 Systematical imaging error by Mirau reference mirror

The measurement noise of CM and WLI was investigated by repeated measurements of a plane mirror. First, 100 measurements were made without changing the mirror position. These images where used to identify z-axis-movement errors through median height values and for identification of the standard deviation of noise signals after correction for z-axis-movements. These errors are explained in detail in section 2.2. After correction for z-axis- movement we investigated the median image of the measurements (seen in Figure 3 left). The median image obviously contains ridges and scratches of up to 10 nm in height. After repeating these measurements at different positions on the mirror with similar results we measured the mirror at over 100 different positions and again used the median height value for each pixel after correction for median height.

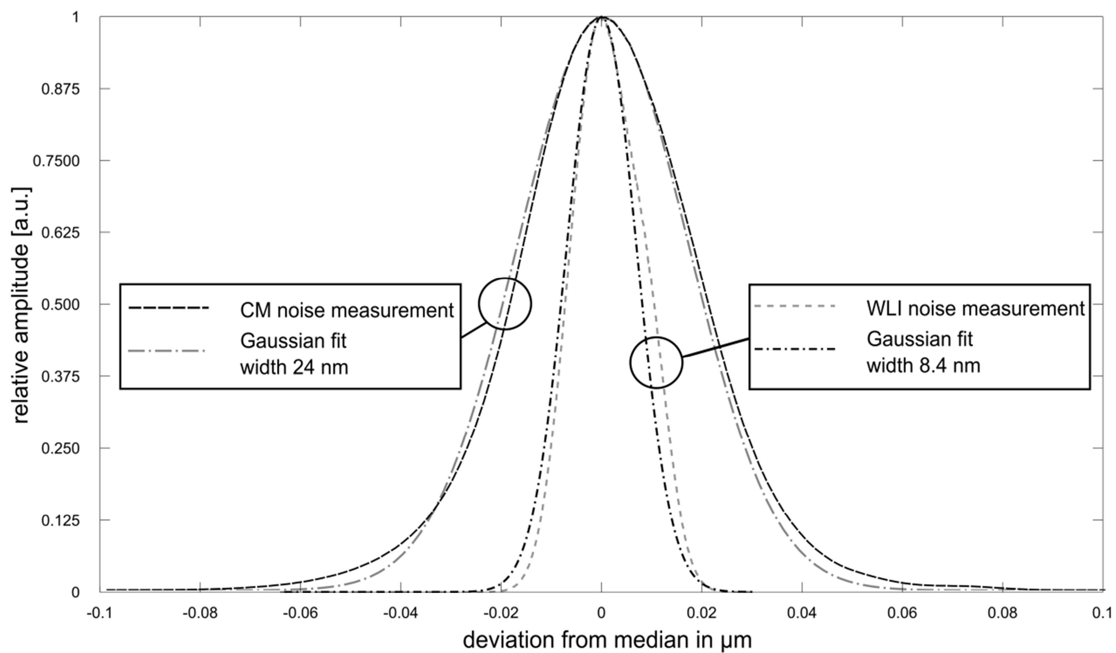

Figure 2: deviations of the median pixel value for 100 measurements of a plane mirror by WLI and CM and Gaussian fits for both distributions

The resulting measurement can be seen in Figure 3 right. This image is obviously the Mirau reference mirror superimposed by the field curvature caused by the lenses. It is necessary to correct all measurements with this image as it is superimposed to all measurements, especially with regard to measurements to be stitched as the field curvature changes the overlap regions. This investigation also shows that measurements at one mirror position are not sufficient as correctional measurements are still influenced by the height structure of the mirror, which is of the same height variation as the errors introduced by the Mirau mirror and the lenses. These measurements allow us to simulate virtual mirror surfaces for calibration purposes and the evaluation of effects of a realistic reference mirror.

Downloaded From: http://proceedings.spiedigitallibrary.org/ on 07/11/2013 Terms of Use: http://spiedl.org/terms

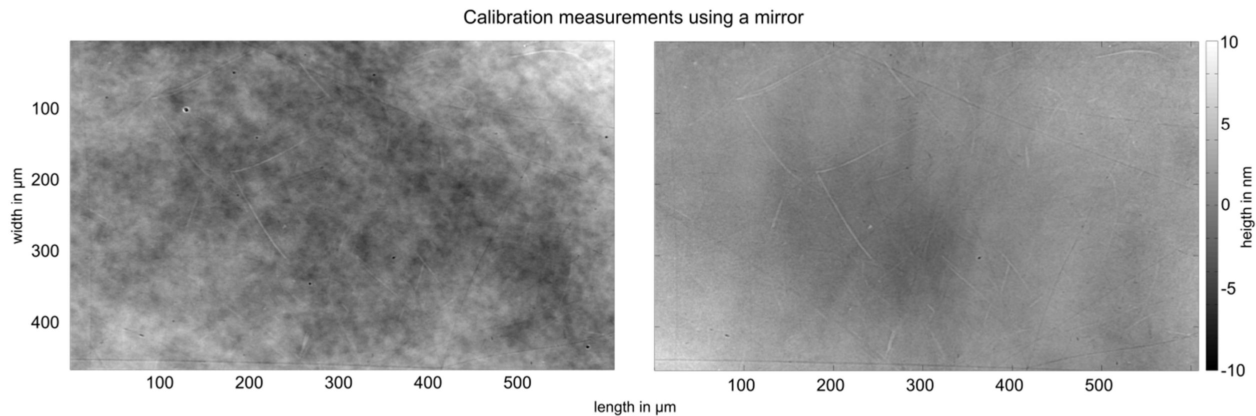

Figure 3: composite measurement of median height values of 100 measurements of a plane mirror using a WLI showing surface effects of the plane mirror and the Mirau reference mirror, 100 times the same mirror position (left), 100 times different mirror positions (right)

3. MOTION ERRORS

The acquisition of measurements for constructing high resolution, high field of view data of technical surfaces requires the translation of either the sensor or the sample with respect to the other. Errors in the positioning can cause great disturbance in the resulting image mosaic if not properly taken into account. We measured the misalignment of the CCD-chip to the translational axis, the repeatability and on axis accuracy of the used positioning stages and the stage drift.

3.1 Misalignment of the CCD-chip

A crucial point in the image acquisition for image mosaics for later fusion by stitching is the correct and automated translation of the sample with respect to the sensor [8]. If the axis of the translation stages are not aligned properly to the sensor the images of the image mosaic contain a rotational deviation. The misalignment of the CCD-chip is easy to discern by measuring repeatedly after translating the sample in a certain direction along one of the translational axis. Each image is registered with respect to the previous image. Any alignment necessary in the direction perpendicular to the axis of movement originates in misalignment of the CCD-chip. The angle between the x-axis of the chip and the x-axis of the stage can be calculated as the arcsine of the quotient of the effective y-translation and the x-translation. By adding additional movements along the second axis this effect can be reduced.

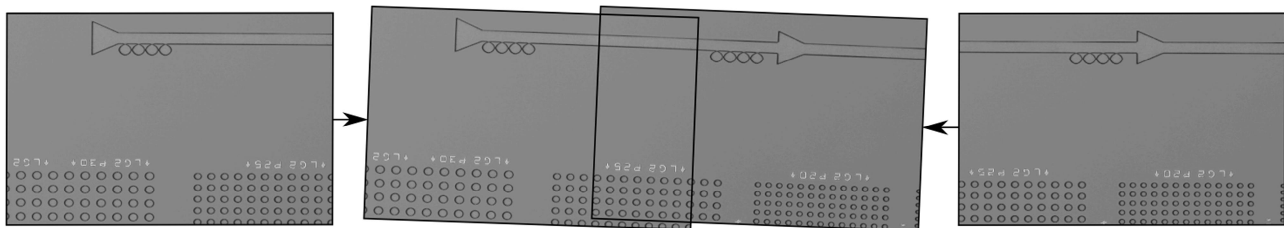

Figure 4: Misalignment of the CCD-Chip with respect to the translational axis, measurements related to one another by translation along x-axis (exterior), image registration shows y-axis translation (interior)

3.2 Repeatability and on axis accuracy

The accuracy with which a certain position along an axis can be achieved is called the repeatability whilst the positional deviation from the axis along the perpendicular axis is called the on-axis-accuracy. To measure these we used a calibration chip and a recognizable target area and performed repeated measurements whilst moving the sample by one third of the field of measurement along one axis, alternating the movement direction. The images are now registered using our algorithm (see section 5) and the spread of coordinates is evaluated. It is important to compensate the angle

Downloaded From: http://proceedings.spiedigitallibrary.org/ on 07/11/2013 Terms of Use: http://spiedl.org/terms

between CCD-chip and movement axis to correctly separate on-axis-accuracy and repeatability. Evaluating 200 movement pairs for different objective lenses we measured a maximum relative axial error for the highest resolution objective (mag. 50x, NA 0.8), with a spread of 20.8 % relative deviation for a 22.48 µm movement with a on-axis error-spread of 345 nm.

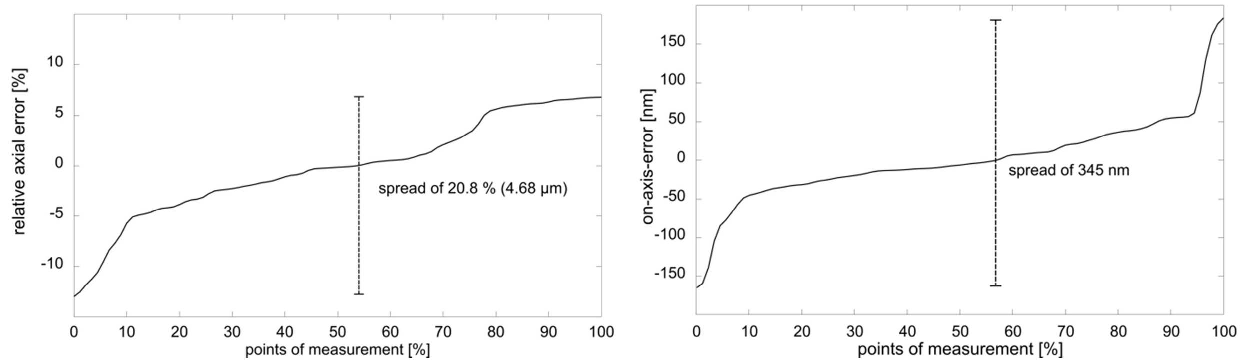

Figure 5: relative axial error for 22.48 µm of movement (left), on-axis-error (right)

3.3 Drift of positioning axis

Drift was measured by using high resolution measurements (numerical aperture 0.8) and a resolution standard. A surface area easy to identify is targeted and periodically measured, then the measurements are registered to the first measurement using correlation by fast fourier transform (CFFT). The median height difference is calculated for each overlap area. With progressing time the position of the surface changes with respect to the measurement volume.

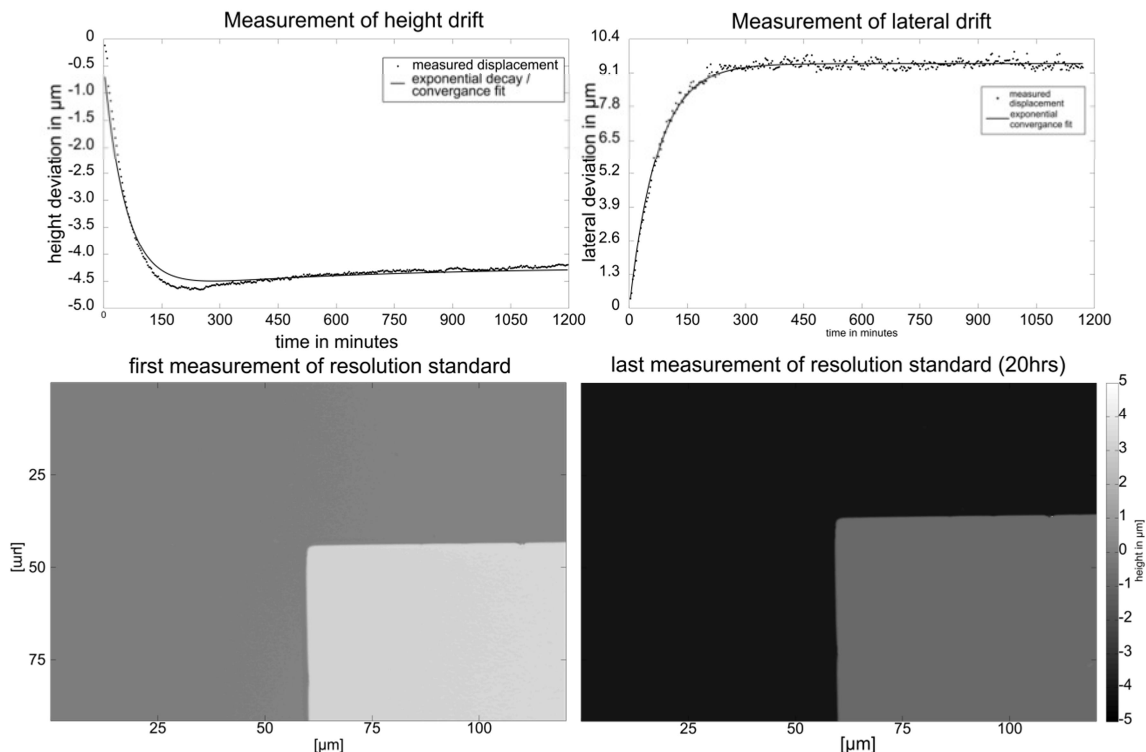

Figure 6: Result of CFFT based image registration of long term measurement of resolution standard (20 hours, measured every 3 minutes, first 15 minutes undocumented (measurement preparation)). Top: measured height drift (left) and lateral drift (right). Bottom: first (left) and last (right) measurement of the series (using the same height scale)

Downloaded From: http://proceedings.spiedigitallibrary.org/ on 07/11/2013 Terms of Use: http://spiedl.org/terms

Measurements were performed for 20 hours every three minutes. In this time the surface to sensor distance changed by 4.3 µm and the target moved by 9.2 µm along the y-axis. The displacement per time is shown in Figure 6. By linearization of the beginning of the drift movements it is easy to calculate the drift speed for y- and z-axis to 2 nm/s and 1 nm/s respectively. Considering the typical measurement time for single stack images of about 0.05 s with a distance between the points of measurement of 20 to 80 nm in height it becomes obvious that the influence of drift is small on single measurements. The lateral drift on the other hand is in the range of 10 to 40 nm per measurement. For high resolution measurements this can be up to a quarter of a pixel, which blurs the measurement. The drift also influences the generation of the image mosaic and leads to necessary alignment corrections.

4. SIMULATIONS

Our goal is to investigate image processing techniques for image alignment and fusion for high resolution, large field of view measurements. To investigate stitching algorithms for 2.5D microscopy without being dependent on special microscopes and surfaces we need generalized imaging systems and surface standards. This is achieved easiest by simulating the surfaces, imaging systems, translation systems and image processing software necessary based on real components.

4.1 Surface Simulation

The simulated surfaces to be measured have a five to ten times higher resolution than the resulting measurements. This is done to allow for the possibility of very rough surfaces, which make the evaluation of surface topography more problematic, as well as subpixel positioning errors which degrade the fusion result. The surfaces are created by random sinus signals with periodicities between two to ten times of the image size for form deviations and one tenth to one of the image size for waviness. The roughness is simulated by a white noise signal with a resolution of twice (for very rough surfaces) to one tenth of the resolution of the generated surface, which is then interpolated using cubic Delaunay interpolation. This simulates different grain sizes and keeps the surface continuous despite the uncorrelated random surface geometry. Finally we simulate polishing of the surfaces by using a histogram based threshold height to cut off higher values and add another Gaussian distributed noise simulating non-uniform polishing and cluttering of valleys by debris caused by the polishing. Sample surfaces can be seen in Figure 7.

The generated surfaces usually have 16 to 56 megapixels to allow for a number of simulated measurements on the same surface. As the surface is effectively down sampled by a factor of 5 to 10 only an area of 1 to 4 megapixels remains available for evaluation of measurement and stitching techniques.

4.2 Measurement Simulation

The measurement simulation is carried out in the following order. First, the measurement path over the surface is calculated, including deviations from the perpendicular grid by CCD chip rotation against the x- and y-axis. In the next step the highest gradients of the surface are calculated based on the height values and the physical resolution of the surface (not to be mistaken for the physical resolution of the optical system!). As the maximum measurable surface angle is dependent on the refractive index and the numerical aperture, not measureable surface pixels are identified by these gradients and these pixels contribute zero intensity to the stack images. Future work will include the use of bidirectional reflactive scattering distribution functions (BRDF) for various surface materials and states [9]. The measurement starts at the lowest point of the desired measuring range and creates a stack image based on eq. 2 (WLI) or eq. 3 (CM) modeled on [10] and [11] respectively.

$$I(z - z_0) = \int_0^\infty S(k) \cos(2kn(z - z_0) + \varphi_0) dk \qquad (2)$$

$$I(z - z_0) = \int_0^\infty S(k) \left[\frac{\sin[kn(z - z_0)(1 - \cos\theta_0)]}{[kn(z - z_0)(1 - \cos\theta_0)]} \right]^2 \qquad (3)$$

Downloaded From: http://proceedings.spiedigitallibrary.org/ on 07/11/2013 Terms of Use: http://spiedl.org/terms

Here I is the intensity in dependenence of the height, $S(k)$ is the spectral density of the used light source in dependence of the wavenumber k, φ_0 is a constant phase, θ_0 is the maximum angle of reflected light, n the refractive index of the surrounding medium, z is the vertical position and z_0 is the height of the surface.

For each step in z-direction a new set of deviations from the optimum positions is generated based on drift, on-axis deviations and jitter. The influence of these for each of the 3 axis involved in objective and sample position can be preset by the user or generated at random based on descriptive parameters. The spectrum of the used lighting can be varied for different measurements and spectral changes due to thermal effects are also easy to implement. After each stack image is generated it is filtered with a Point-Spread-Function with a width based on the axial distance of the surface from the focus position to simulate light scattering. As the resolution of the stack image is still higher than physically possible, the now filtered stack image is down sampled by averaging over 25 to 100 pixels to generate the measurement stack image used for evaluation by the virtual microscope. By this means we incorporate problems due to missing intensity contributions, which result in missing values (NANs). The evaluation of the stacks is performed using parabolic fitting of the intensity stack or the envelope of the intensity or a fit of a sinus signal enveloped with a Gaussian, as eq. 3 would suggest for a Gaussian formed spectral density in a WLI.

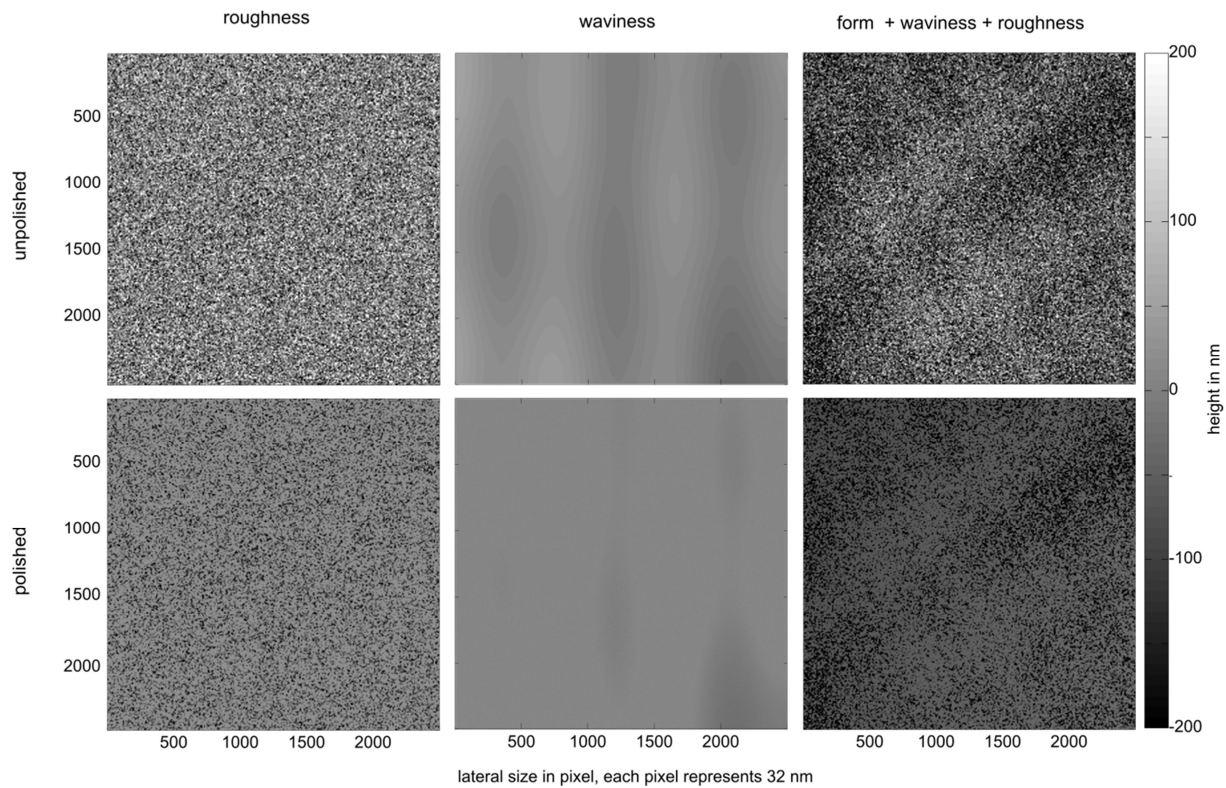

Figure 7: Set of sample surfaces generated by our method, incorporating roughness trough Gaussian noise and interpolation as well as waviness and form by sine signals with varying frequencies. The second row shows the surfaces in the first row after our polishing simulation. Each image is 2500 by 2500 pixels and represents a measurement area for 500 by 500 pixels each of which represents 160 nm.

Downloaded From: http://proceedings.spiedigitallibrary.org/ on 07/11/2013 Terms of Use: http://spiedl.org/terms

5. IMPROVED IMAGE ALIGNMENT BY CORRELATION USING FAST FOURIER TRANSFORMATION THROUGH 1D-FEATURE FUNCTIONS

5.1 Correlation by fast fourier transformation (CFFT)

Correlation is a standard method for image registration but computationally expensive. Using the convolution theorem for fourier transformation in two dimensions a computationally cheap method for image registration becomes available [7]. For large overlaps the correlation function by fast fourier transform (eq. 4) becomes a sharp peak. As the convolution by fourier transform uses periodic boundaries the correlation function becomes more complicated as the overlap between the convoluted images shrinks. Also prior knowledge of the translation direction is necessary due to the periodic boundary condition. In microscopic image stitching we generally have knowledge of the translation direction so CFFT is applicable. As mentioned before the overlaps between bordering images of the mosaic need to be relatively large (50 to 30 percent), which increases the time for measurement of the surface drastically. To alleviate this problem we developed an algorithm to minimize the window size of the convoluted images roughly to the actual overlap.

$$C(x,y) = F^{-1}\{F\{I_1(x',y')\}.* F^*\{I_2(x'',y'')\}\} \quad (4)$$

Here $C(x,y)$ is the unnormalized cross-correlogram, $F\{f\}$, $F^{-1}\{f\}$ and $F^*\{f\}$ the discrete fourier transform of f, its inverse and the complex conjugate respectively and $.*$ the element wise multiplication.

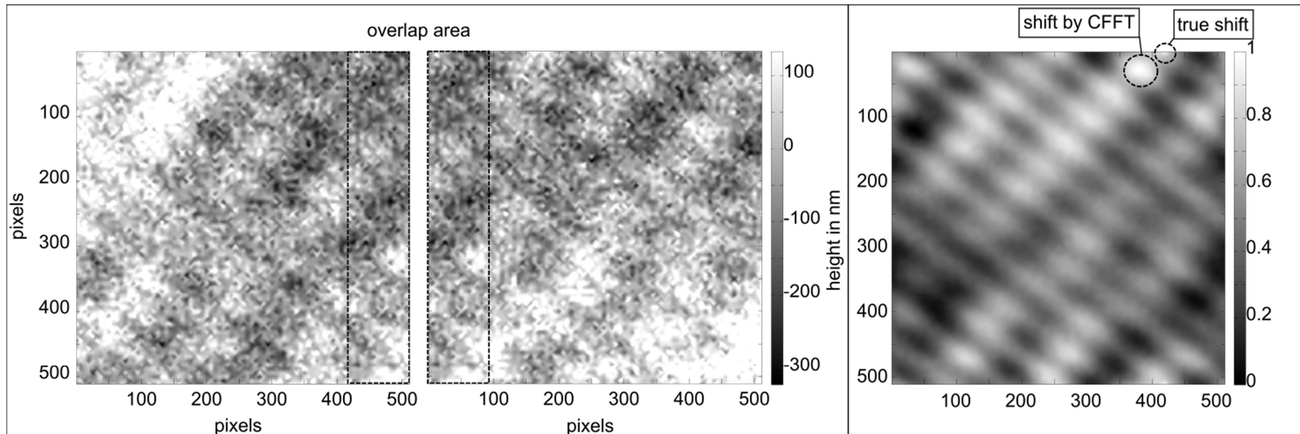

Figure 8: Overlapping simulated measurements with 18% overlap (left) and their cross-correlogram by CFFT (right)

5.2 Algorithm

Image registration techniques that use integral intensity along columns and rows of images have been investigated in the past [12, 13]. In commercial WLI and CM the measurements usually are exported not as intensity image stacks but rather as already evaluated height matrices. Using integral height along rows and columns is more dependent on height changes due to drift and, if used, the auto focus repositioning but can also be used for quick image registration. As stitching of measurement sets by WLI and CM is purely translational, aside from optical distortions, the correlation by fast fourier transformation (CFFT) is a fast and noise robust method for image registration that can also be applied to 2.5D data. But CFFT is of limited use once the overlap area percentage becomes small. The registration accuracy decreases for larger translations, usually at 40% to 20% overlap area. By restricting the area of the images compared to one another this effect can be countermanded, but it requires prior knowledge of the overlap area. We developed the idea of image registration based on integral height along the columns for pure translations along the row axis to incorporate other types of functions based on the height distribution along the columns. By adding other functions of the height values we increase the available information for the registration process without needing the entire image and thereby decreasing the computing time compared to cross correlation. We use the standard deviation, the maximum and the minimum along the columns as well as the same functions based on the gradients perpendicular to the columns. By minimizing the square difference of the normalized translated functions for both images we are able to find the overlap area, though true registration is not achieved as the loss of information by restricting us to 8 functions is too high. By including more feature functions, based on surface curvature and periodicity for example, the accuracy of the algorithm could be

Downloaded From: http://proceedings.spiedigitallibrary.org/ on 07/11/2013 Terms of Use: http://spiedl.org/terms

increased at the cost of computing time. As the estimation of the overlap by our algorithm is very robust we use it to decrease the area of the height matrices used for CFFT and then compose the true alignment coordinates by the two data as it is currently more time efficient as well as robust against noise. Using our algorithm on simulated measurements we were able to register images using CFFT with overlap areas of 7% and higher (Figure 9). Interestingly the algorithm works best on simulated measurement data overlaid with noise as described in section 2.2. This might be the result of aliasing effects of the simulated surfaces with respect to the down sampling by the measurement simulation and needs further research to increase the effectiveness of our simulation.

5.3 Results of simulation

We performed simulated WLI measurements of overlapping surface areas of 10 simulated surfaces by stepwise decreasing the overlap from 50% to 0% and registered the resulting measurements using traditional CFFT and our algorithm (Figure 9).

We used a radial distortion as measured with our CM (section 2.1), overlaid the images with noise as high as our CM, used a scratched Mirau reference mirror represented by an "LUH" of 10 nm in height, the CCD-Chip was rotated against the translational axis by 6° (section 3.1), used an on-axis-accuracy with a 5% percent spread (section 3.2) and a lateral drift of $1/\sqrt{2}$ pixels per image measurement (section 3.3). The results show a clear increase in accuracy for small overlaps down to 7% of the image size.

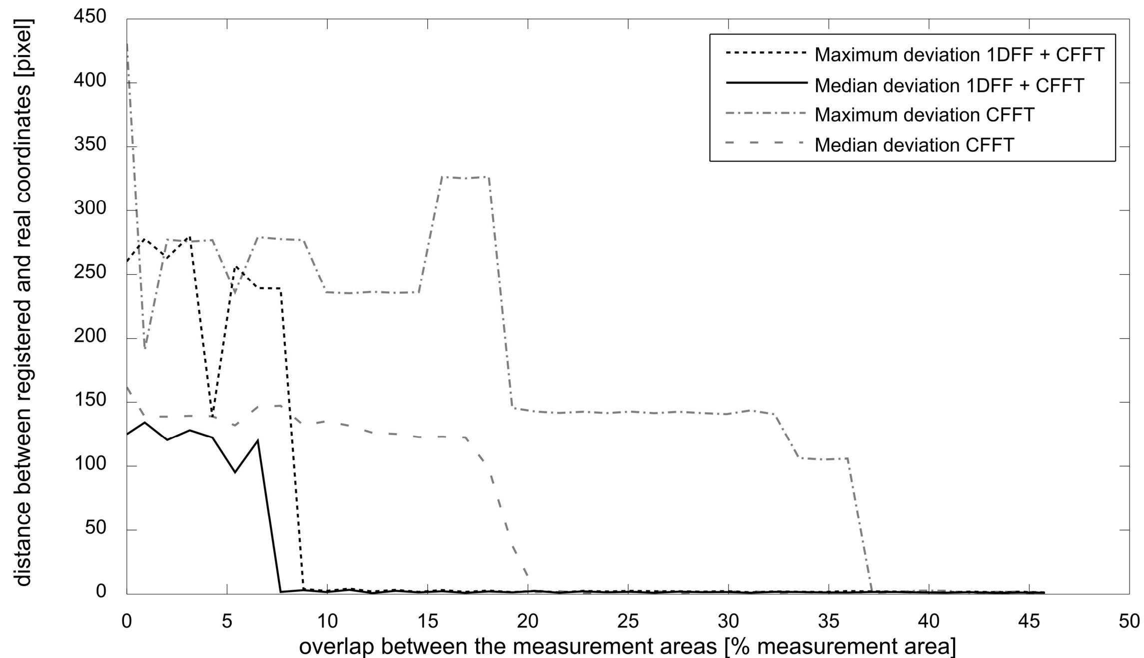

Figure 9: comparison of shifts found by CFFT and 1D-feature functions followed by CFFT (1DFF + CFFT)

6. SUMMARY AND OUTLOOK

We developed a simulation of microscopic imaging using white light interferometers and confocal microscopes using realistic optical, processing and positioning error sources for the simulation of image mosaic measurements for later stitching of measurement data. We used this simulation to create measurement data of simulated technical surfaces which we used to evaluate an algorithm developed by us to increase the usability of correlation by fast fourier transformation, by decreasing the necessary overlaps down to 8% of the image size. This is done by preregistering the images using 1D feature functions of the intensity along image columns.

Downloaded From: http://proceedings.spiedigitallibrary.org/ on 07/11/2013 Terms of Use: http://spiedl.org/terms

We will incorporate more complex models for the microscopes and surfaces to resemble real optics and surfaces more closely, implement sample material based parameters like dispersive refractive indices and BRDF like light scattering and use the simulation to test other algorithms for image registration, in example SURF based or mutual information algorithms.

7. AKNOWLEDGEMENT

This work was financed by the “Deutsche Forschungsgemeinschaft” as part of the project “Datenfusion optisch flächenhaft erfasster Mikrotopografien mit Bezugsebene” (Data fusion of optically measured micro topographies with plane of reference).

REFERENCES

[1] Shaw, L. and Weckenmann, A., "Automatic registration method for hybrid optical coordinate measuring technology," CIRP Annals-Manufacturing Technology, 60(1), 539-542 (2011).

[2] Sjo, M. and Oreb, B. F., "Stitching interferometric measurement data for inspection of large optical components," Optical Engineering, 41(2), 403-408 (2002).

[3] Fleischle, D., Lyda, W., Gronle, M., Mauch, F., Körner, K., & Osten, W., "Herausforderungen und Lösungsansätze für die fertigungsnahe Qualitätskontrolle mittels optischer 3D-Messtechnik," tm-Technisches Messen, 80(1), 3-8 (2013).

[4] Holme, B., & Lunder, O. "Characterisation of pitting corrosion by white light interferometry," Corrosion science, 49(2), 391-401 (2007).

[5] Vallance, R. R., Morgan, C. J., Shreve, S. M., & Marsh, E. R., "Micro-tool characterization using scanning white light interferometry," Journal of micromechanics and microengineering, 14(8), 1234 (2004).

[6] Brown, D. C., "Close-range camera calibration," Photogrammetric engineering, 37(8), 855-866 (1971).

[7] Szeliski, R. [Image alignment and stitching: A tutorial - Foundations and Trends® in Computer Graphics and Vision 2, no. 1], now Publishers Inc., Hanover, MA, 1-104 (2006).

[8] Hao, Q., [Optische 3D-Erfassung und Auswertung technischer Oberflächen hinsichtlich ihres Verschleißverhaltens], Shaker Verlag, Aachen, 27-55 (2011)

[9] Krauss, M., Kästner, M. and Reithmeier, E., "Evaluation of Worn Surfaces Using Directional Illumination," Proc. 5th Int.Conference on Optical Measurement Techniques for Structures & Systems 2012, 195-203 (2013).

[10] Lehmann, P., "Vertical scanning white-light interference microscopy on curved microstructures," Opt. Lett. 35, 1768-1770 (2010)

[11] Mauch, F., Lyda, W., Gronle, M., and Osten, W. "Improved signal model for confocal sensors accounting for object depending artifacts," Optics Express, 20(18), 19936-19945 (2012).

[12] Cain, S. C., Hayat, M. M., & Armstrong, E. E. "Projection-based image registration in the presence of fixed-pattern noise." IEEE Transactions on Image Processing, 10(12), 1860-1872 (2001).

[13] Guthier, B., Kopf, S., Wichtlhuber, M., Effelsberg, W , "Parallel algorithms for histogram-based image registration," 19th IWSSIP, 172-175 (2012)

Downloaded From: http://proceedings.spiedigitallibrary.org/ on 07/11/2013 Terms of Use: http://spiedl.org/terms